RESEARCH ARTICLE

Super-Resolution Imaging by Computationally Fusing Quantum and Classical Optical Information

Randy A. Bartels¹, Gabe Murray², Jeff Field¹, and Jeff Squier³

¹Department of Electrical and Computer Engineering, Colorado State University, Fort Collins, CO 80523, USA. ²Department of Physics, Colorado State University, Fort Collins, CO 80523, USA. ³Department of Physics, Colorado School of Mines, Golden, CO 80401, USA.

*Address correspondence to: randy.bartels@colostate.edu

A high-speed super-resolution computational imaging technique is introduced on the basis of classical and quantum correlation functions obtained from photon counts collected from quantum emitters illuminated by spatiotemporally structured illumination. The structured illumination is delocalized—allowing the selective excitation of separate groups of emitters as the modulation of the illumination light advances. A recorded set of photon counts contains rich quantum and classical information. By processing photon counts, multiple orders of Glauber correlation functions are extracted. Combinations of the normalized Glauber correlation functions convert photon counts into signals of increasing order that contain increasing spatial frequency information. However, the amount of information above the noise floor drops at higher correlation orders, causing a loss of accessible information in the finer spatial frequency content that is contained in the higher-order signals. We demonstrate an efficient and robust computational imaging algorithm to fuse the spatial frequencies from the low-spatial-frequency range that is available in the classical information with the spatial frequency content in the quantum signals. Because of the overlap of low spatial frequency information, the higher signal-to-noise ratio (SNR) information concentrated in the low spatial frequencies stabilizes the lower SNR at higher spatial frequencies in the higher-order quantum signals. Robust performance of this joint fusion of classical and quantum computational single-pixel imaging is demonstrated with marked increases in spatial frequency content, leading to super-resolution imaging, along with much better mean squared errors in the reconstructed images.

Citation: Bartels RA, Murray G, Field J, Squier J. Super-Resolution Imaging by Computationally Fusing Quantum and Classical Optical Information.

Intell. Comput. 2022;2022:Article 0003. https://doi.org/10.34133/icomputing.0003

Submitted 19 September 2022 Accepted 2 November 2022 Published 21 December 2022

Copyright © 2022 Randy Bartels et al. Exclusive licensee Zhejiang Lab. No claim to original U.S. Government Works. Distributed under a Creative Commons Attribution License 4.0 (CC BY 4.0).

Introduction

Imaging makes use of light captured from an object to quantify information about the structure and function of the object. The ability to discern spatial features in optical imaging is dictated by the information content contained in the light captured from the object [1]. Information content is limited by the properties of propagating radiation when the light used to form an image is collected in the far field. The primary constraint imposed by light propagation is referred to as the diffraction limit, which imposes a spatial resolution restriction on the order of the optical wavelength λ . This is because spatial frequencies higher than $1/\lambda$ decay exponentially in amplitude when propagating away from an object. A revolution is under way in optical microscopy where the quantum properties of light are exploited to extract additional information from quantum correlations that are absent in the classical interpretation [2]. Such quantum information brings new possibilities but also its own set of limitations. Here, we develop a broader computational imaging approach to fuse quantum and classical information to provide a general solution that jointly exploits both forms of information for superresolution microscopy.

Over the past few decades, numerous super-resolution microscopy methods have emerged that circumvent the optical diffraction barrier by bringing new information into the measurements [3]. This new content is injected by exploiting photophysical properties such as structured illumination [4,5], localization [6], saturated absorption [7], or coherent nonlinear scattering [8,9]. These super-resolution imaging techniques treat the total light signal collected during the image exposure time classically, and thus, information content is consequently restricted.

In fact, additional imaging information can be accessed on the basis of fluctuations of the optical signals emitted by the object or, alternatively, imparted onto the illumination (excitation) beam [10,11]. Correlations in the emitted light from an object can be exploited for scalable enhancements in imaging resolution—provided that those temporal fluctuations can be measured. Typically camera integration times (greater than milliseconds) are sufficiently long such that fluctuations of the emitted light intensity are essentially averaged to undetectable levels under many circumstances. The temporal fluctuations of photons detected in an optical signal depend on the nature of the emitters, the emitter environment, the integration time, and the detector configuration.

We focus our attention on self-luminescent emitters, such as fluorescent molecules, quantum dots, or color centers, such as nitrogen vacancies in nanodiamonds. In the case of luminescent objects, the collected light lacks spatial coherence, which means that the light emitted at distinct spatial locations add together through an incoherent intensity sum upon detection. Single quantum emitters exhibit emission intensity fluctuations on 2 relevant time scales, with classical correlations encompassing times greater than microseconds and quantum correlations occurring on submicrosecond times [12]. Intensity fluctuations can happen when the emitter is removed from the population, either temporarily as occurs with quantum dot blinking or molecular photoswitching, permanently because of photobleaching, or during the waiting period for re-excitation of the emitter to the excited state after photon emission.

Specifically, on longer time scales, quantum emitters can exhibit fluctuations (blinking) of photon emission due to intermediate trapping in dark (off) states. Such classical fluctuations are impacted by the local environment of the quantum probes, and as such, the rates of these dynamics can vary by orders of magnitude, ranging from microseconds to minutes. The statistics of classical temporal fluctuations in photon emission are useful for computational super-resolution imaging. To extract information from these fluctuating signals, a new image signal is obtained by calculating correlations (or auto and cross cumulants) between the detected signal photons. For conventional imaging methods, the information content from light intensity fluctuations is limited by the statistics of classical light [10,13].

On shorter time scales (submicrosecond), the light fluctuations are often quantum in nature. Recently, new approaches have been introduced that exploit nonclassical light to enable super-resolution imaging [2]. The essential quantum property that is responsible for super-resolution microscopy [14] is exquisitely simple: a single quantum emitter can only emit 1 photon at a time as this emission only occurs when the emitter is in an excited state. This key property of single-photon emission produces a decidedly nonclassical correlation in the photon state. Correlations of detected photons from a single emitter will have a null at zero delay between photons, a property called antibunching. Such anti-bunching quantum correlations can be exploited to distinguish between the spatial location of independent quantum emitters. Quantum anti-bunching correlations are particularly useful because of their robustness under experimental conditions (e.g., temperature, losses, and scattering). In contrast, classical fluctuations experienced by emitters depend sensitively on the local environment around the emitter, resulting in perturbations that range over orders of magnitude, depending on the local experimental conditions.

Anti-bunching correlations are observed in all sorts of single quantum emitters (atoms, ions, molecules, and quantum dots) [12,14,15] on time scales that are short compared to classical temporal fluctuations [12]. When more than 1 quantum emitter has a reasonable probability for detection in the collected imaging signal, then individual emitters may be distinguished through the anti-bunching correlation on the basis of the Glauber correlation functions. These correlation functions, given by $G^{(k)}(t_d=0)=\left\langle\prod_{i=0}^{k-1}\left(\widehat{n}-i\right)\right\rangle$ at zero time lag $t_d=0$, can be used to build an image model that confers super-resolution properties. Here, \widehat{n} is the number

operator. Traditional classical information is directly provided by the first-order correlation function $G^{(1)}(0) = \langle \hat{n} \rangle$, which is simply the mean photon count recorded during the integration time of the detector.

Ultimately, the goal of anti-bunching super-resolution imaging is to ascertain the spatial location of the emitters by counting photons from these emitters extracted from analyzing quantum Glauber correlation functions. Quantum correlation experiments are run in a photon-counting mode, and the desired correlations can then be post-selected. The first experimental implementation [16] used a straightforward method for building an anti-bunching quantum imaging instrument that incorporated a photon-counting capable camera combined with the pulsed excitation of single quantum emitters [16]. Pulsed excitation ensures that, at most, only 1 photon can be emitted by a quantum emitter per excitation. By restricting the pump pulse frequency to the frame rate of the camera, direct counting of photons emitted by the sample is achieved. The magnification of the microscope was designed such that the point spread function (PSF) was oversampled by the sensor pixels of the camera. Such oversampling allows adjacent pixels to serve as detectors for photons emitted simultaneously from different emitters within the PSF. This, in turn, enables the estimation of a quantum super-resolution antibunching image so that individual emitters now appear out of a single PSF volume. Unfortunately, imaging rates are limited by long camera integration times due to relatively slow (~ kHz) frame rates. Confocal detection enjoys faster (megahertz compared to kilohertz) photon counting rates offered by singlepixel photon-counting modules (SPPCM), but the illumination and detection must be scanned across every point within the object [17]. When SPPCMs are configured with a set of beam splitters, second- and higher-order Glauber correlation functions can be estimated, providing anti-bunching image signals. Alternately, a high-speed single-photon-sensitive camera can be assembled from a fiber bundle arrayed with SPPCMs [18–20] or a single-photon avalanche diode array [21]; the field of view, but field of view, and thus imaging speed, remains limited.

A subtle limitation is evident in these experiments: the quantum-correlation super-resolution comes at a price [16,17]. That cost is that only a fraction of the detected photon counts can be used for image formation. The impact of such postselection of photon counts is that much of the collected information is discarded for the quantum super-resolution image. In this Article, we introduce a new computational imaging strategy that fuses the quantum and classical information to provide high-quality imaging that exploits the best of both the quantum and classical worlds. This new approach uses anti-bunching correlation images combined with classical images derived from the same photon-count data. With this strategy, the shortcomings of anti-bunching quantum superresolution microscopy techniques are averted. In addition, we introduce a new strategy for high-speed quantum antibunching super-resolution imaging by adapting a classical imaging strategy that used spatiotemporally structured light to illuminate an extended spatial region with a series of spatial frequency projections [9,22-26]. By using high-speed SPPCMs to allow for the extraction of quantum correlations from structured-illumination single-pixel imaging, we introduce new quantum super-resolution capabilities. Specifically, we develop and demonstrate a computational imaging strategy that integrates the best features of the quantum and classical

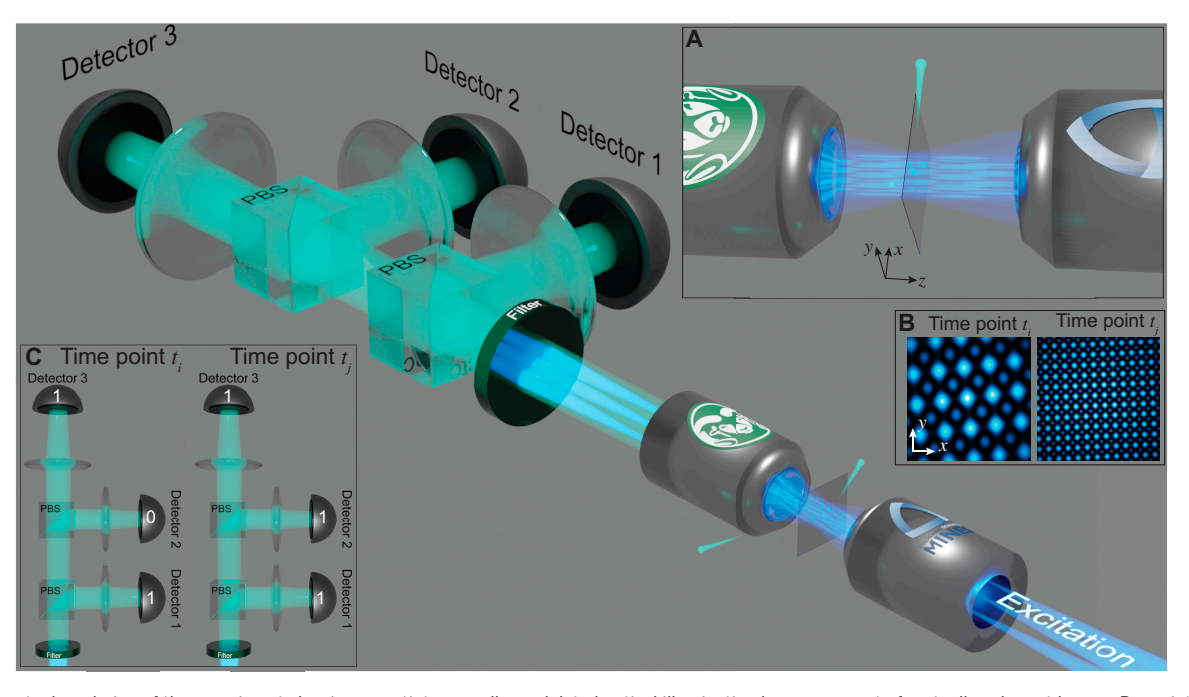


Fig. 1. Conceptual rendering of the experiment showing a spatiotemporally modulated optical illumination by a sparse set of mutually coherent beams. Beam interference produces the spatially structured illumination as illustrated in the main figure and insets (A) and (B). A large focal volume is achieved because each beam encompasses a small region of spatial frequency support in the pupil plane. The center spatial frequency of the beams scans across the pupil, cycling through a set of complex illumination patterns with spatial frequency structure the samples the full numerical aperture (NA) of the illumination objective lens throughout the full temporal modulation cycle. The figure shows an unfolded microscope; however, epi detection is possible. Detection efficiency could be improved by combining photon coincidence counts in multiple directions. (A) A zoomed-in example of the structured illumination light intensity at 1 time sample. The specimen is placed in the region of the slide. (B) The spatial structure of the illumination intensity in the plane of the slide for 2 time points. (C) Examples of generalized HBT detection showing cases of 2 and 3 simultaneous photon detection events.

imaging modalities. The strategy is simple to implement because the classical and quantum signals are directly extracted from a single data stream: the set of photon counts from highspeed single-photon-counting detectors. To robustly fuse the high signal-to-noise ratio (SNR) but low-spatial-frequency information from the classical information with the lower SNR, but higher-spatial-frequency information from the quantum correlations, we developed a new computational imaging algorithm to jointly deconvolve the data from various orders of quantum and classical images and simultaneously improve the image SNR across a broad spectrum of spatial frequencies. This approach benefits from the redundancy in overlap of information across lower spatial frequency regions. In particular, the low-spatial-frequency content that is common to all of the imaging modalities must be self-consistent. This selfconsistency requirement enforces a greater accuracy in the image estimation of the higher spatial frequency content from the quantum information. The result is that high-speed, superresolution images with high SNR can be obtained with our fusion of computational quantum-classical image information, which we refer to as super deconvolution imaging (SDI).

Methods

New imaging information from nonclassical correlations

To facilitate high-speed super-resolution imaging with quantum correlations, we combine temporally structured illumination with single-pixel photon-counting detection for computational imaging. A generalized Hanbury Brown–Twiss (HBT) detection

strategy enables estimation of the number of photons emitted by the specimen for each excitation pulse (see Fig. 1). The changes in spatial structure of the illumination light is indexed by φ , which evolves in time, and from which the image is estimated computationally. A set of photon counts captured from $N_{\rm bin}$ excitation pulses for a given illumination light spatial structure with time index φ is used to compute zero-delay Glauber correlation functions. To simplify the description, we adopt the notation for the correlation around φ of $G^{(k)}(t_d = 0) \to G_0^{(k)}(\varphi)$. The classical image signal $S^{(1)}(\phi)$ is simply the mean number of detected photoelectrons, which is proportional to the number of detected photons $\langle \hat{n} \rangle (\phi) = G_0^{(1)}(\phi)$. Higher-order statistical processing of the photon-count data to obtain correlation functions for k > 1 reveals quantum anti-bunching correlations that are otherwise hidden (or lost) in the photon counts. Thus, by computing higher-order correlation functions, indexed by k, quantum images can be extracted from the single-photoncount dataset, as shown in Fig. 2.

As noted, anti-bunching is a distinct hallmark of single quantum emitters that can be, and has been, exploited for super-resolution imaging [14,16–18,27]. The essential quantum computational imaging information is gleaned from the Glauber correlation functions computed from measured photon counts from which anti-bunching effects from quantum emitters are extracted. We are specifically interested in the correlation function at zero delay, $t_d = 0$. For a photon emitted at a time $t_d = 0$, it is not possible for another photon to be emitted from the same emitter. The ability to detect a second photon from this emitter is conditioned on the emitter being, once again, promoted to the excited state. In addition, there is

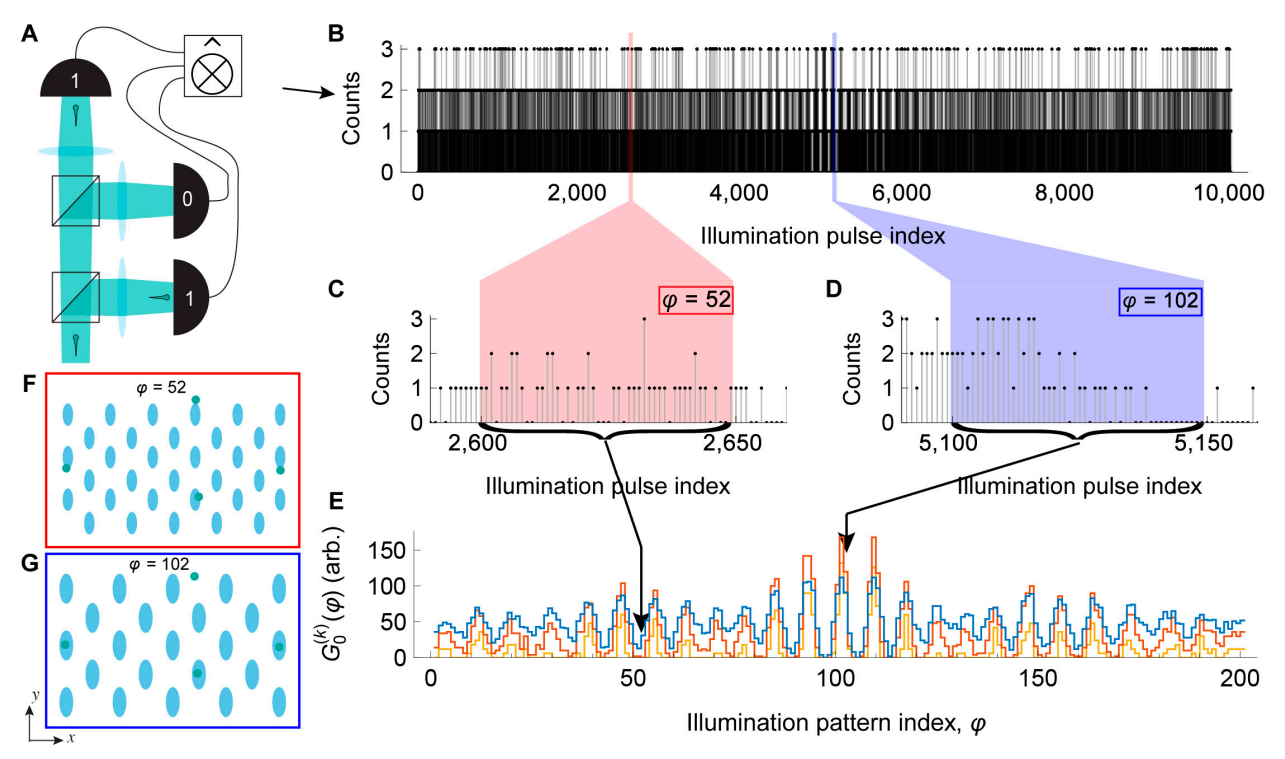


Fig. 2. Illustration of the computation of Glauber correlation functions from the number of detected photon counts after each excitation pulse. Each group of photon counts from which the correlation functions are computed correspond to a particular spatial illumination pattern. (A) Modified HBT detection for estimating the number of detected photons recorded during each excitation pulse cycle. (B) Monte Carlo simulation of the number of photon counts produced by 3 emitters for each excitation pulse. The emission probability for each emitter is proportional to the spatiotemporal illumination intensity pattern at the location of that emitter. Photon emission is modeled as a Bernoulli process with an event occurrence probability determined by the excited-state population using the photo-physical model described in the text. (C and D) Examples of the subselection of the population of detected photons for 2 spatial patters occurring over N_{bin} pulses. (E) Un-normalized, zero-delay Glauber correlation functions, $G_0^{(K)}(\varphi)$, for k = 1,2,3 are computed from the photon counts binned for consecutive sets of N_{bin} detected photon numbers centered on a structured intensity index φ , as illustrated by the shaded regions examples for φ_a and φ_b . (F) and (G) illustrate the 2 illumination intensity patterns, $I_n(x,\varphi)$, at a particular times indicated by φ . These examples are shown in 2 dimensions for clarity and highlight specific examples appearing in the photon counts for N_{bin} pulses. Each illumination pattern can excite a subset of the emitters. The number of detected photons for a given excitation pulse number is modulated by the excitation probability for each illuminated emitter, the direction of photon propagation, and losses and inefficiencies in the detectors. In (F), 3 of the emitters are partially illuminated, whereas in (G), 3 emitters are strongly illuminated. Images are constructed by exploiting the known spatial illumination patterns at each φ point in the Glauber corre

a time interval that the emitter must wait before another photon is emitted after the emitter returns to the excited state. The net time scale thus depends on the spontaneous emission rate and the pumping rate. Consequently, at zero time delay, $t_d=0$, the normal-ordered Glauber correlation function of light emitted by a single quantum emitter vanishes, $G^{(2)}(t_d=0)$. This behavior is a reflection of the simple fact that the emitter is not capable of immediately emitting another photon. Here, we will be using the normalized Glauber correlation function $g^{(k)}(t_d) = G^{(k)}(t_d)/(G^{(1)}(0))^k$.

In contrast, when photon emission can be collected from multiple quantum emitters (within a single detection volume), the emitters emit light independently, and even if the emitters exhibit correlations at some initial time, say during excitation, the emitters dephase rapidly, which is evident in the broad emission bandwidth of an uncorrelated ensemble of quantum emitters. Thus, a large number of emitters exhibits a net emission that is completely uncorrelated, so that the correlation function is simply the mean photon count, $g^{(2)}(t_d) \rightarrow 1$. However, for the case where a small number of emitters are contained within the detection volume, the correlation function can be written as $g^{(2)}(0) = 1 - 1/N$, which is simply a consequence of the fact that after 1 emitter has released a photon, there are (N-1) remaining emitters that can also produce a photon. Here, we see that in the limit of large $N, g^{(2)}(\tau) \rightarrow 1$ [15].

The factors that influence the photon detection probability are illustrated in Fig. 1 and are determined by the photon emission, p_e , and photon collection, p_o probabilities. As these probabilities are uncorrelated, the total detection probability is simply the product of these probabilities, $p_d = p_e \times p_c$. The emission probability depends on both the photophysical properties of the emitter and by the spatial distribution of the optical illumination that excites the emitter, which for our purposes will be controlled by resonant optical excitation. In contrast, the collection probability is determined by the size and configuration of the optical detector and the collection optical system.

For incoherent light emitted by an ensemble of quantum emitters, we may describe the probability of light detection as the product of the total collection efficiency, η_t , and with the image transfer function probability density function, $h(\mathbf{x}_d, \mathbf{x}_o)$, where \mathbf{x}_o and \mathbf{x}_d are the object and detection plane transverse coordinate, respectively. The total collection efficiency is the product of the detector quantum efficiency, the collection efficiency of the optical system, and the total intensity transmission through all optical components. The collection probability is then obtained from the spatial integral across the spatial domain, D, of the photodetector, leading to $p_c(\mathbf{x}_i) = \eta_t \int_D h(\mathbf{x}_d, \mathbf{x}_o) d^2\mathbf{x}_d$. The collection probability for single-pixel computational imaging is determined by the experimental arrangement but can

generally be expressed as a constant $p'_c(\varphi) = \eta_c$ that depends on the efficiency of collection optics and detectors. The limited efficiency of collection does not impact the single-pixel computational imaging model, so we will focus on the emission probability.

In order for a given emitter to release a photon, the emitter must be in the excited state, $|e\rangle$. In an imaging experiment, a population of emitters in the object will be illuminated (see Fig. 2F and G) and some fraction of those emitters will be promoted from the ground to the excited state. Assuming pulsed optical excitation, we may estimate the excited-state population by solving for the population kinetics. The probability of excitation depends on the local illumination intensity, which we write in with unit intensity magnitude as $I_n(\mathbf{x}_o, t)$, and the excited-state population may be related to the illumination intensity through a nonlinear function, $F[\cdot]$, in the case of saturated or multiphoton absorption. The illumination intensity and physical properties of the emitter determine the emission probability, $p_e(\mathbf{x}_o, t) = k_r | e(\mathbf{x}_o, t) \rangle$. For an emitter in the excited state at some time t, the rate of photon emission can be generally modeled with first-order rate kinetics, as an exponentially decaying probability density with a decay time constant of the emission rate, k_r .

A model for the multiphoton state produced by a set of independent quantum emitters can readily be constructed by assuming lossless detection. This assumption only modifies the rate of photon counting without distorting the quantitative forward model. If we were restricted to a single emitter, labeled by *j*, then the number operator for the detected photon state is simply $\hat{n}_i = \hat{a}_i^{\dagger} \hat{a}_j$. The density operator for this single-photon

state,
$$\hat{\rho}_j = \left(1 - p_e^j(\mathbf{x}_{o,j})\right) |0\rangle\langle 0| + p_e^j(\mathbf{x}_{o,j}) |1\rangle\langle 1|$$
, depends on

the probability of emission p'_e for an emitter positioned at loca-

In imaging, there will generally be more than 1 emitter with a nonzero detection probability. The expected number of detected photons is given by $\langle \hat{n} \rangle = \text{Tr} \{ \hat{\rho} | \hat{n} \}$, where the total number operator, $\hat{n} = \sum_{i} \hat{n}_{i}$, for the multimode photon state produced by an ensemble of N quantum emitters described by the density operator for the multiphoton state of $\hat{\rho} = \bigotimes_{i=1}^{N} \hat{\rho}_{i}$. With a large ensemble of excited quantum emitters, the random fluctuations reduce to a statistical ensemble, and thus only classical correlations are observed, with all quantum correlations obscured. We require that the number of excited states are small enough so that the anti-bunching signal can be experimentally discerned.

Hybrid quantum-classical computational imaging with sinusoidally structured illumination: forward model

A key requirement for computational imaging is the existence of a high-quality, computationally efficient forward model. Here, we provide the models for both the quantum anti-bunching and classical forward imaging techniques. We focus on spatiotemporally structured illumination with a pulsed laser source [9]. In the typical scenario, the excitation pulses are simultaneously several orders of magnitude shorter than the luminescence lifetime of the emitters and the period between pulses is at least 4 to 5 times larger than this same temporal relaxation time. These conditions ensure that, with high probability, only 1 photon may be emitted by each emitter for each pulse. As we have discussed, the collection probability is constant across emitters, so that we now only need to establish a quantitative model for the variation of the emission probability within the spatiotemporally modulated illumination intensity.

The probability of emitted light for pulse excitation is driven by the peak excited-state population. Following excitation of an emitter by a pump pulse arriving at time t_0 with a pulse duration, $T_{\rm pu}$ much shorter than the excited-state lifetime, τ_e , so that $T_{\rm pu} \ll \tau_e = (k_{\rm r} + k_{\rm nr})^{-1}$, the excited-state population decays exponentially, $|e(\mathbf{x}_o,t)>=e_m \exp{(-[t-t_0]/)\tau_e})$ for $t\geq$ t_0 , from the peak excitation probability e_m . Here, k_{nr} is the nonradiative decay rate. Thus, while the probability of the excited-state population, and thus the emission probability, decays exponentially after pulsed excitation, the total probability of emission after pulsed excitation for a single quantum emitter is equal to the peak excited-state population, e_m .

The peak excitation probability e_m depends on the illumination intensity impinging on the emitter. We consider pulsed illumination with a peak intensity that varies across the object coordinate as $I_{\text{ill}}(\mathbf{x}_o, \varphi) = I_{\text{max}} I_n(\mathbf{x}_o, \varphi)$. The global maximum for the illumination intensity is denoted as I_{\max} so that I_n is the structured illumination intensity with the peak intensity normalized to unity. The excited-state probability varies in space and time because of the nonlinear map, $F[\cdot]$, from the normalized illumination intensity to the emission probability $e_m =$ $F[I_n](\mathbf{x}_o, \varphi)$. Here, φ denotes a time-dependent variation on the illumination intensity. In the case of short pulse excitation considered here, the excitation function is $F[\cdot] = 1$ $\exp[-\gamma_{\rm pu}I_n(\mathbf{x}_o,\varphi)]$. The peak emission probability also scales with the pump saturation parameter $\gamma_{pu} = \alpha_0 (T_{pu}/\tau_e)$ and where $\alpha_0 = I_{\text{max}}/I_{\text{sat}}$, with I_{sat} denoting the emitter saturation intensity.

Because the collection geometry (see Fig. 1) is such that the photon emission is collected uniformly from across the object spatial distribution, the detection probability from a set of emitters is $p_d^{(\varphi)} = p_c \int e_m(\mathbf{x}_o, \varphi) c_\sigma(\mathbf{x}_o) d^2\mathbf{x}_o$, where c_σ is the surface concentration for a 2-dimensional distribution of quantum emitters. If we consider a discrete set of emitters located at the points \mathbf{x}_j , then $c(\mathbf{x}_o) = \sum_j \delta(\mathbf{x}_o - \mathbf{x}_j)$. Measured photon counts may be processed to compute the

normalized Glauber correlation functions (see Fig. 2) from which we extract quantum correlations for super-resolution imaging. Modulation pattern-dependent signals extracted from the k^{th} -order signal can be adapted from previous expressions [14,17,27] to give a signal of the form

$$S^{(k)}(\varphi) = \left\langle \hat{n} \right\rangle^k(\varphi) \, y^{(k)}(\varphi), \tag{1}$$

where $y^{(k)}(\varphi)$ is a polynomial function that depends on the order k. These polynomial functions are easily derived using the density matrix of the multiphoton state. The first 2 orders are $y^{(2)}(\varphi) = 1 - g_0^{(2)}(\varphi)$ and $y^{(3)}(\varphi) = 1 - (3/2) g_0^{(2)}(\varphi) + (1/2) g_0^{(3)}(\varphi)$. Here, we define the zero-delay correlation functions for the spatial structured illumination pattern indexed by φ as $g_0^{(k)}(\varphi) = G_0^{(k)}(\varphi) / \left[G_0^{(1)}(\varphi) \right]^k$.

$$\varphi \text{ as } g_0^{(k)}(\varphi) = G_0^{(k)}(\varphi) / \left| G_0^{(1)}(\varphi) \right|^k$$

Previous anti-bunching imaging experiments used the signals given in Eq. 1 as the estimates of the images. Extension of anti-bunching super-resolution imaging to quantum computational imaging requires a new approach. The recorded signal model is $S^{(k)}(\varphi) = \int \left[p_d^{(\varphi)}(\mathbf{x}_o) \right]^k d^2\mathbf{x}_o$. With the pulsed model of the excitation probability, this model can be rewritten as $S^{(k)}(\varphi) = (\Phi p_c)^k \int c_\sigma(\mathbf{x}_o) F^k [I_n(\mathbf{x}_o,\varphi)] d^2\mathbf{x}_o$. In this new approach, we derive classical information from k=1 and quantum information from the higher orders, k>1.

Considering a specific scenario in which a modulated line focus with a geometry set by $\mathbf{x}_o = (x, y)$ is employed [22,26], with a normalized intensity given by $I_n(\mathbf{x}_o, \varphi) = \rho(y)(1 + \cos[\Xi])^2/4$, where $\Xi = \omega_c \varphi + 2 \pi \kappa x \varphi$ and $\rho(y)$ is the intensity distribution perpendicular to the line focus. A simplified expression can be obtained from a cosine series expansion of $F^k[\cdot]$, so that our signal becomes

$$S^{(k)}(\varphi, y) = \sum_{q = -\infty}^{\infty} \tilde{S}_q^{(k)}(\varphi, y) \exp(-i \omega_c \varphi).$$
 (2)

The cosine expansion terms simply read

$$b_q^{(k)}(\varphi,y) = \frac{1}{2} \int F^k \big[I_n \big(\mathbf{x}_o, \varphi \big) \big] \, \cos \big[q \, \Xi \big] \, d\Xi.$$

Classical and quantum images may now be estimated from the set of demodulated signals

$$\tilde{S}_{q}^{(k)}(\varphi, y) = (\Phi p_{c})^{k} \int c_{\sigma}(\mathbf{x}_{o}) b_{q}^{(k)}(\varphi, y) \exp\left[-iq2\pi \kappa x \varphi\right] d^{2}\mathbf{x}_{o}.$$

The signals shown in Fig. 2E are the extracted photon counts collected from a sweep of the illumination modulation pattern for a given position of a line focus illumination [9] or several line cursors [28]. Referring to Eq. 3, we see the object that we wish to recover is related to the signal from a set of projections that are manifested in the signal orders q, k. Each signal term, q, in the $k^{\rm th}$ -order cosine expansion then provides additional super-resolution orders as we previously established for classical single-pixel structured illumination [9]. Processing of the signal traces in Fig. 2E produces a set of line images. A full image is built from scanning the line focus, but speed is improved compared to confocal imaging due to the reduced number of scan points required.

Each of the signals for a given k and q can be represented as an estimated image from 1 photon-count dataset. The estimated image that takes the form of a convolution, $\hat{c} = c_{\sigma} * \mathrm{PSF}_q^{(k)}$, of the desired object, c_{σ} with the PSF for the given image order. The PSF for the $(k, q)^{\mathrm{th}}$ order is directly obtained from the cosine expansion coefficients using an inverse Fourier transform with respect to the modulation spatial frequency in the φ^{th} illumination pattern $f_x^{(\varphi)} = \kappa \varphi$, leading to $\mathrm{PSF}_q^{(k)}(\mathbf{x}_o) = \int b_q^{(k)}(\varphi,y) \exp\left(i\,2\,\pi\,x\,q\,f_x^{(\varphi)}\right)\,\mathrm{d}f_x^{(\varphi)}$.

SDI to fuse quantum and classical information

The detection of photon counts from spatiotemporally modulated illumination provides a set of images that span over a set of indices of the photon correlation order, k, and the cosine expansion order of the nonlinear excitation, q. It is evident from Eq. 3 that higher resolution (higher spatial frequency content) is contained in the higher-order (k, q) terms. In addition, we see that since Φ , p_c < 1, the higher-order terms drop in intensity. Thus, the resolving power of this imaging strategy is limited by the noise as the signal drops for higher-order

expansion terms. We have developed a computationally efficient joint deconvolution strategy to fuse the super-resolution imaging information from the set of quantum and classical images that can be extracted from the signal vectors in Eq. 3. This SDI strategy benefits from the requirement of selfconsistency of information obtained across the ranges of spatial frequency information support that increases with higher expansion orders. The computational imaging problem here is one where we seek to fuse the information from both quantum and classical images that are well-modeled by a linear convolution model to estimate the object c_{σ} . While this can be viewed as a simple problem of minimizing the difference between the measured data and the estimated signal derived from the estimated object, the challenge is that the large set of images that need to be jointly deconvolved lead to an intractable numerical computation problem if we seek to solve the problem directly. Consequently, we have developed a computationally efficient algorithm that avoids the instantiation of large matrices in computer memory that would be required for directly solving this problem.

The data for each image are obtained from the collected photon counts such as shown in Fig. 2B. These counts are based on a Monte Carlo simulation of photon emission from a set of 3 quantum emitters. Photon counts for each excitation pulse are plotted. The set of photon counts are binned, with $N_{\rm bin}=50$, and the zero-lag Glauber correlation functions, ${\bf G}^{(k)}(0)$, are computed (as displayed in Fig. 2C). Using Eq. 3, discrete signal models, ${\bf y}^{(k)}=\tilde{\bf S}_q^{(k)}+\epsilon_q^{(k)}$, are obtained. All of these vectors are obtained from statistics extracted from each set of $N_{\rm bin}$ detected pulse counts that are converted into the signal terms using Eq. 1. The variable $\epsilon_q^{(k)}$ is a noise vector. Each of the noise-free demodulated signal vectors are modeled as a linear correlation with the discrete PSF matrix operator, ${\bf A}_q^{(k)}$, as $\tilde{\bf S}_q^{(k)}={\bf A}_q^{(k)}$ c. The vector ${\bf c}$ is the discrete form of the object that we wish to estimate.

The set of signal data from the classical, k=1, and quantum $1 < k \le K_{\max}$ image orders, for each of the modulation expansion orders $q \in \{1, ..., q_{\max}\}$ leads to a large set $(J=q_{\max}K_{\max})$ of images. We will index elements of this entire set with the subscript j. To jointly solve for the underlying object estimate using the full set of image data, we concatenate the signals into 1 long vector $\mathbf{y}_T = \{\mathbf{y}_1|\cdots|\mathbf{y}_J\}$. Each signal is of length N_s , so that the total concatenated vector is J N_s . Similarly, we concatenate the convolution matrices to form \mathbf{A}_T . The goal is to estimate the object by formulating the problem as a least mean squared fit

$$\mathbf{c}^* \coloneqq \underset{\mathbf{c} > 0}{\operatorname{argmin}} \frac{1}{2} \left(\|\mathbf{A}_T \ \mathbf{c} - \mathbf{y}_T\|_2 + \|\lambda I \ \mathbf{c}\|_2 \right). \tag{4}$$

We make use of forms of gradient descent to solve our problem, which requires the computation of the adjoint of \mathbf{A}_T . Because of the size of \mathbf{A}^T and \mathbf{A} , matrix computations using these matrices are not feasible. Instead, we observe that the adjoint of the convolution is a cross correlation and that the operation of these large matrices can instead be efficiently computed using fast Fourier transform operations. As the object estimated must first be padded along the concatenation direction, the resulting cross correlation is cropped to recover the adjoint operation.

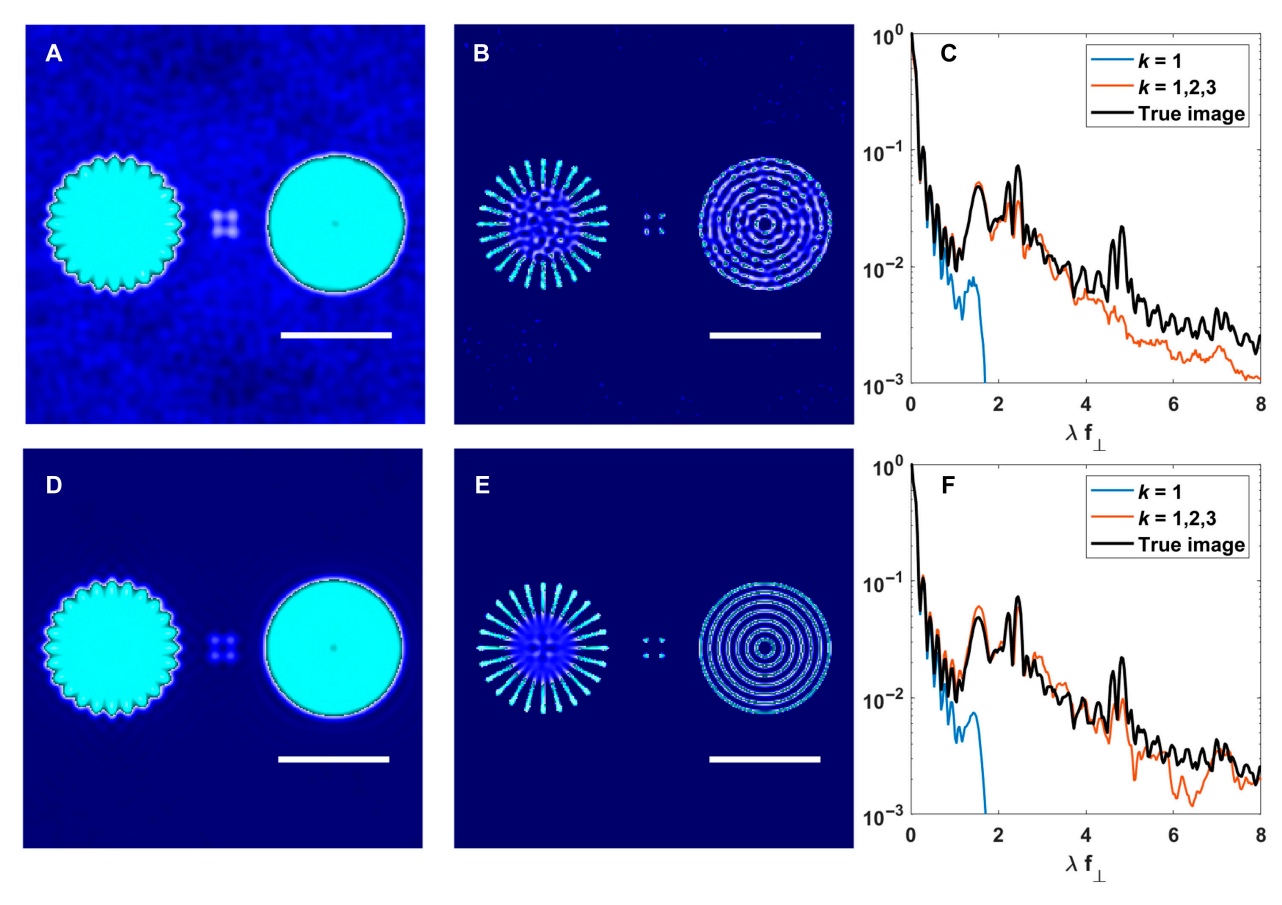


Fig. 3. Results of the joint deconvolution algorithm fusing both classical and quantum information for linear absorption. Insets (A) and (D) are the highest-resolution images using classical information (k=1, q=2) for a mean photon count levels $\overline{n}=500$ a) and $\overline{n}=5\times10^6$ (D). Insets (B) and (E) combine both classical and quantum image orders (k=1,2,3) also for mean photon count levels $\overline{n}=500$ (B) and $\overline{n}=5\times10^6$ (E). Inset (C) and (F) show the radial average of the Fourier transform of the reconstructions compared to the actual image used in the simulation for photon count levels of $\overline{n}=500$ (C) and $\overline{n}=5\times10^6$ (F). Scale bar is 5λ .

Results

Simulations of joint SDI image estimation fusing classical and quantum information were implemented for mean photon counts ranging 7 orders of magnitude from $\overline{n} = 5$ to $\overline{n} = 5 \times 10^6$. In a photon counting regime, noise in the measurement can be accurately described with Poissonian statistics. While imaging resolution is often discussed as an absolute property that is determined by the properties of an optical instrument, that is only part of the story. The optical instrument does determine the PSF; however, it is impossible to determine spatial resolution without knowledge of the SNR levels. All imaging methods exhibit an imaging resolution that is constrained by the SNR. Our strategy extracts more information from a dataset than is possible with conventional imaging strategies, because both classical and several orders of quantum anti-bunching images are obtained. While each of these images exhibits an SNR that limits imaging resolution, when the sets of quantum and classical images are jointly deconvolved, the new estimated images displays a vastly improved SNR. Because we are performing simulations, the true SNR performance may be directly validated.

In Figs. 3 and 4, we see simulated images for both low and high mean-photon-count levels. The test image is based on Siemens spoke test pattern, a radial grating, and a cluster of 4 points. We show the classical image at the low and high photon

counts, along with the joint quantum-classical image for k =2&3 Glauber correlation functions. It is evident that the joint information extracted from the exact same dataset from the SDI algorithm applied to the quantum and classical images is far superior to the simple classical image. The intuition that higher spatial frequency content is available is more readily apparent in the radially averaged spatial frequency content from the images that is shown in Figs. 3C and F and 4C and F. Here, we see that the simple classical image information drops precipitously above a normalized transverse spatial frequency of $\lambda f_{\perp} > 2$. By contrast, in the joint quantum-classical estimated image, the transverse spatial frequency support is maintained across the full relevant spatial frequency band. Similar trends are observed for both the 1- and 2-photon absorption cases; however, the 2-photon case displays better absolute resolution as one expects [9].

Example calculations for low photon counts for 1 photon imaging are in Fig. 4A to C and for the 2-photon case in Fig. 4A to C. The classical cases are both shown in panels A of the figures. In the linear (1 photon absorption) excitation case, virtually no spatial features are resolved (Fig. 3A), which can be seen in the radially average spatial frequency trace for k = 1 in Fig. 3C. Similarly, for the low-photon-count case with the nonlinear (2-photon absorption) excitation case, some spatial features are resolved but are buried in the noise (Fig. 4A), and still, the radially averaged spatial frequency support

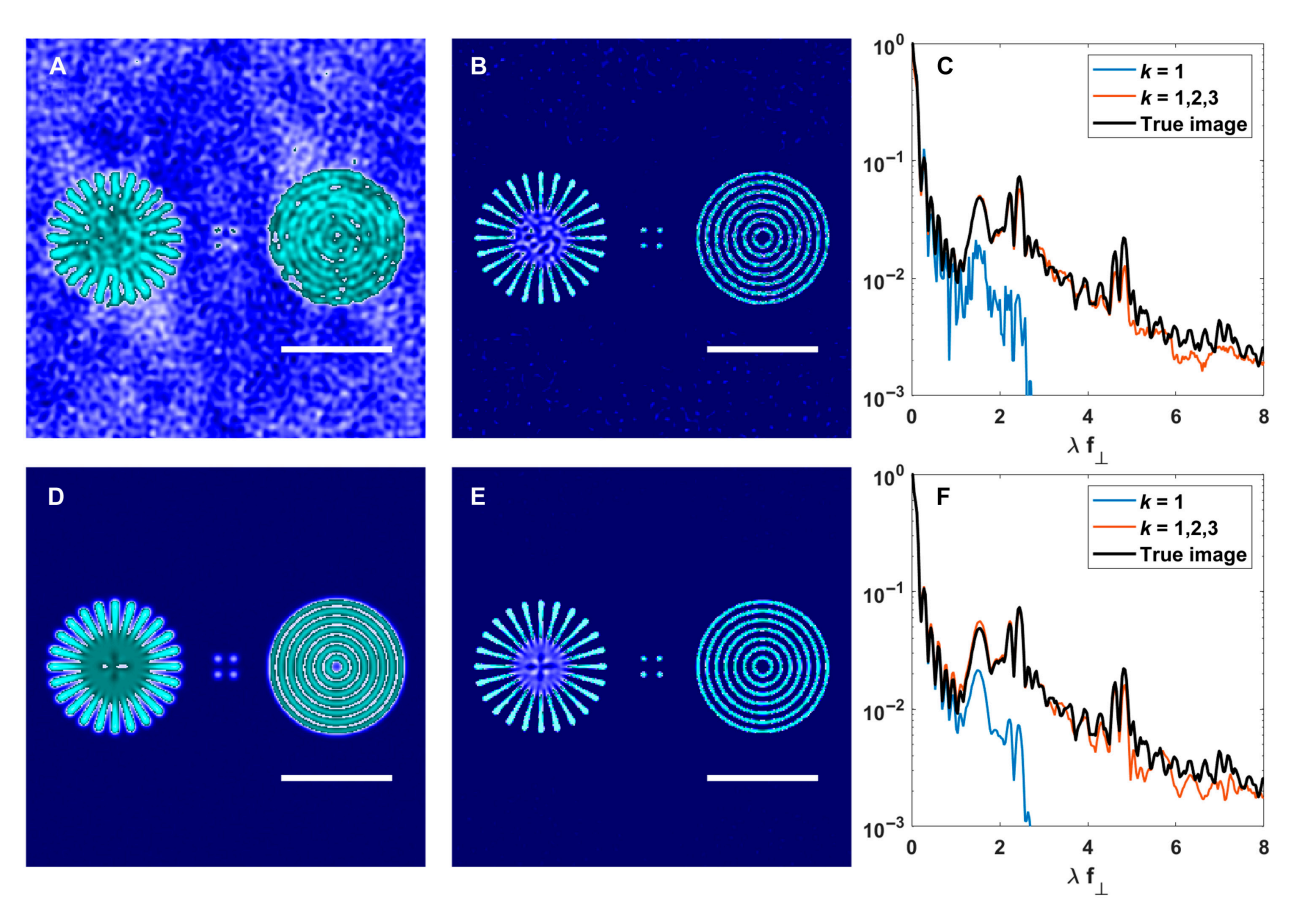


Fig. 4. Results of the joint deconvolution algorithm fusing both classical and quantum information for 2 photon absorption. Insets (A) and (D) are the highest resolution images using classical information (k = 1, q = 4) for a mean photon count of $\overline{n} = 500$ (A) and $\overline{n} = 5 \times 10^6$ (D). Insets (B) and (E) combine both classical and quantum image orders (k = 1,2,3) also for mean photon counts of $\overline{n} = 500$ (B) and $\overline{n} = 5 \times 10^6$ (E). Inset (C) and (F) show the radial average of the Fourier transform of the reconstructions compared to the actual image used in the simulation for mean photon count levels $\overline{n} = 500$ (C) and $\overline{n} = 5 \times 10^6$ (F). Scale bar is 5λ .

is poor as shown in k=1 in Fig. 4C. Taking the signals derived from second- and third-order Glauber correlations to produce quantum images (k=2,3), along with the classical image (k=1), the resultant application of SDI to that full set of images produces a high-quality image with low noise as shown in Figs. 3B and 4B for the 1- and 2-photon absorption cases, respectively. The improved image quality is evident in the radial spatial support in the C panels. The lower rows in Figs. 3 and 4 show the results of SDI applied to a high average photon count case. As expected, the noise is low in all cases, we also see that in the classical case, image features are still poorly resolved, whereas the joint quantum-classical reconstructions shows high image quality with a near perfect match between the ideal and reconstructed radially averaged spatial frequency support.

The quality of the image obtained from the data can be computed from the mean squared error (MSE), defined as MSE = $N^{-1} \sum_{i=1}^{N} (X_i - X_i^*)^2$ where N is the total number of elements, X is the true image, and X^* is the image estimated from the data. In Fig. 5, we provide the MSE for a wide range of algorithm performance conditions, where we investigate classical, quantum, and joint computational imaging strategies for a wide range of mean photon count levels. The classical case failed for the case of $\overline{n} = 5$, while the joint quantum-classical SDI reconstruction still yielded an MSE of 0.0595 for 2PA and 0.0707 for 1PA, so Fig. 5 starts at $\overline{n} = 50$. The variation

in mean photon count also severely impacts the SNR of the data. Because there are a wide array of possible classical images that we can extract from the spatial frequency orders, q, to reduce the dimensionality of the data, we report the best MSE across all q values for the classical case. The MSE for quantum-only image estimates is treated similarly, and finally the joint deconvolution using SDI is shown.

Conclusion

In general, super-resolution microscopy techniques make use of additional information that can be accessed with either the manipulation of the excitation process for an imaging probe or by exploiting the properties of the emitted light. Antibunching super-resolution microscopy is a promising new direction that exploits quantum correlation from single quantum emitters [14]. Previous experimental anti-bunching imaging systems suffered from low imaging rates. We introduce a new strategy for high-speed anti-bunching super-resolution microscopy based on the illumination of the sample with a temporally varying sequence of spatially structured illumination light. While this spatiotemporally structured light illumination strategy enjoys the benefits of the highest-speed photon-counting detectors and faster imaging than point-bypoint confocal scanning, this quantum imaging strategy still has the limitation of the quantum anti-bunching super-resolution

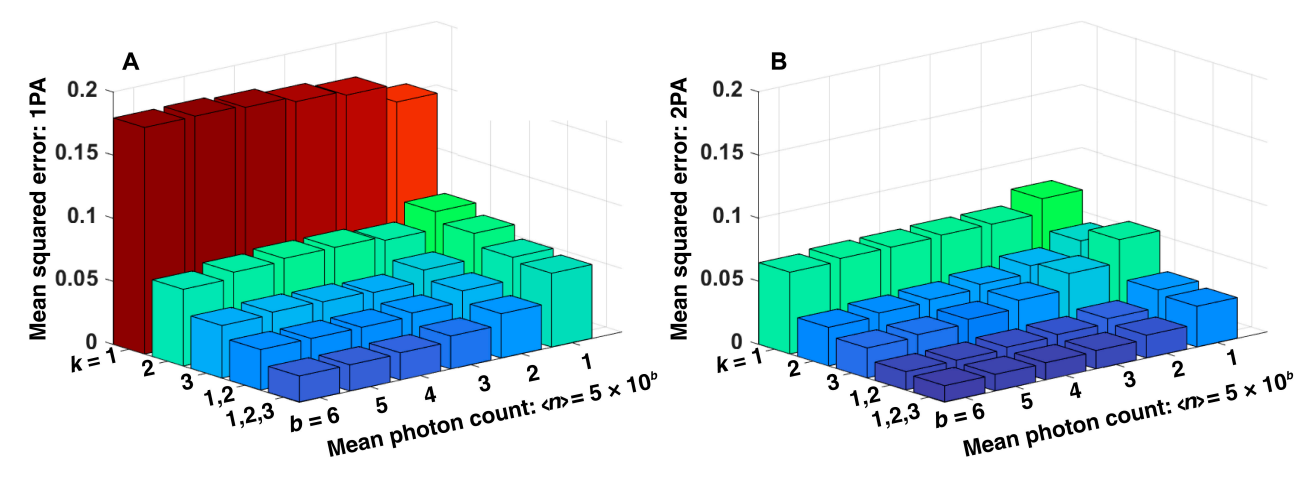


Fig. 5. MSE for image reconstructions using signal orders (k = 1, k = 2, k = 3) and joint SDI of the combined quantum and classical information (k = 1, 2 and k = 1, 2, 3) for linear (1PA) (A) and 2 photon absorption (2PA) (B) across many different photon count levels. For each correlation order, the lowest MSE across the corresponding set of images (indexed by q) is reported. The classical case is restricted to k = 1. Quantum images are derived from k = 2, and k = 3. The joint SDI images are given for the sets of k-values: k = 1, 2 and k = 1, 2, 3 which include all corresponding q values. For the linear absorption SDI case including correlation orders k = 1, 2, 3 there are a total of 12 images which have been jointly deconvolved and 24 for TPA case. Using correlation orders k = 1, 2, 3 there is a total of 6 and 12 images for 1PA and 2PA respectively.

microscope: the reduced total photon counts from the post-selected correlation functions. The lowest-order correlation function (k=1) is restricted to classical information and thus cannot improve the spatial resolution by using the quantum correlations that are present in higher-order correlation functions. Unfortunately, the number of counts that contribute to successively higher signals drops by at least an order of magnitude between successive correlation signal orders k [16,17]. Thus, higher-spatial-resolution information suffers from a reduced SNR at increasingly larger correlation orders.

The drop in SNR of high-spatial-frequency information is an important challenge observed in anti-bunching quantum images that are post-selected from second- and higher-order Glauber correlation functions. This means that, while the quantum anti-bunching images contain more information on very small, and thus high, transverse-spatial-frequency features, the SNR is lower than the classical counterpart that is obtained from the first-order correlation function. We have developed an algorithm that fuses the high SNR information available in the quantum information with the lower SNR information from the higher-order quantum signals. The spatial frequency content from each of the set of images is jointly deconvolved with the PSF of each of the images obtained from the photon-count data. Because all of the images contain information that overlaps in lower spatial-frequency ranges, and because the same underlying object is being probed, the algorithm exploits the requirement of self-consistency of the overlapping measured spatial frequency information to bootstrap the lower SNR information at high spatial frequencies that is contributed by the quantum images. Of particular utility here is that from 1 dataset, we can derive a large number of images from classical, and then various orders of quantum correlations. Thus, our strategy is able to extract substantially more information from a single measurement, optimizing the information content extraction obtained from the measurement. Notably, the fusion of classical and quantum information boosts the SNR of the image that is retrieved from the algorithm. Our SDI algorithm is extremely versatile as it does not require a-priori information about the object, such as sparsity [20]. All that is

required is the set of images extracted from the classical and quantum information in the data to be combined with an estimate of the imaging PSF for each modality. On the basis of this set of information, our efficient SDI algorithm fuses the information from the multiple imaging modalities. By enforcing self-consistency between the regions of spatial frequency information overlap, we produce a high-SNR super-resolution image based on this synthesis of quantum and classical information. Our algorithm only requires a set of images with known PSFs and thus can be used in any imaging system that obtains multiple images from a set of measurements. While prior object information is not required if such prior information does exist, it can be used to good advantage as a regularization in the image reconstruction algorithm.

In addition to the fusing of classical and quantum information, our new quantum computational imaging approach uses a previous strategy of classical super-resolution imaging method that we demonstrated for computational single-pixel superresolution imaging [9,26]. As a result, we exploit 2 co-operative mechanisms for improving the imaging resolution: antibunching and nonlinear generation of addition spatial frequency harmonics. These 2 resolution enhancement pathways result in broadened spatial frequency support, as depicted in Figs. 3 and 4. A common feature of super-resolution microscopies is that the higher-spatial-frequency information is obtained at the price of reduced SNR in that information. The fusion of both the multiple pathways for high-spatialfrequency information enables a substantially higher SNR in the images than would be possible by directly using a single super-resolution image.

Another advantage brought by our approach is improved imaging speed. Our strategy adapts a single-pixel computational super-resolution imaging modality to exploit anti-bunching to exploit quantum correlations for enhanced super-resolution imaging. The single-pixel detection structured-illumination strategy that we use here is called SPIFI (for SPatIal Frequency modulation for Imaging) [22]. The fact that SPIFI uses spatiotemporally structured illumination enables an extended illumination region, while being able to exploit the $\sim 10^7 - 10^9 \times \text{faster}$

photon counting rate of single-pixel photon-counting detectors. This development makes the best of both worlds of previous anti-bunching imaging by simultaneously making use of spatially extended illumination and high-speed photon counting. The previous disadvantages of slow camera photon counting in widefield illumination [16] or point detection that requires slow scanning to form an image [17].

A further practicality of our strategy is that our approach can be implemented in existing multiphoton laser scanning microscopes simply with the introduction of a cylindrical lens and a modulator disk [29] and the use of time-correlated singlephoton detection. As a result, existing laser scanning microscopes can be readily upgraded to extend the imaging resolution of those systems. The fusion algorithm that we present here has much wider application than this particular imaging modality. The widespread utility rests on the simplicity of the algorithm: that this provides an approach for computationally efficient joint deconvolution of a set of images of 1 object that are captured with a set of diverse PSFs and may be described with a standard convolutional model of imaging [1]. Example applications where the SDI algorithm could provide advantages include SAX imaging [7] and various correlative microscopies. Because of the multiple aspects where both the imaging modality for quantum-classical single-pixel imaging and the general strategy for obtaining an image of an object that is probed by diverse imaging modalities, we anticipate widespread use of the techniques demonstrated in this work.

Acknowledgments

Funding: This work was supported by the National Institutes of Health (NIH) (R21EB025389 and R21MH117786) and the National Science Foundation (NSF) (1707287). **Author contributions**: R.A.B., J.F., and J.S. conceived the research. R.A.B. wrote the Monte Carlo simulations for photon counts and image simulation. G.M. and R.A.B. developed the SDI algorithm. All authors wrote the manuscript. **Competing interests**: The authors declare that they have no competing interests.

Data Availability

Additional data and materials are available online.

References

- Mertz J. Introduction to optical microscopy. 2nd ed. Boston (MA): Cambridge Univ. Press; 2019.
- 2. Moreau P-A, Toninelli E, Gregory T, Padgett MJ. Imaging with quantum states of light. *Nat Rev Phys.* 2019;1(6):367–380.
- Pujals S, Feiner-Gracia N, Delcanale P, Voets I, Albertazzi
 L. Super-resolution microscopy as a powerful tool to study complex synthetic materials. *Nat Rev Chem.* 2019;3(2):68–84.
- 4. Heintzmann R, Huser T. Super-resolution structured illumination microscopy. *Chem Rev.* 2017;117(23):13890–13908.
- 5. Balzarotti F, Eilers Y, Gwosch KC, Gynnå AH, Westphal V, Stefani FD, Elf J, Hell SW. Nanometer resolution imaging and tracking of fluorescent molecules with minimal photon fluxes. *Science*. 2017;355(6325):606–612.
- Möckl L, Moerner WE. Super-resolution microscopy with single molecules in biology and beyond–essentials,

- current trends, and future challenges. *J Am Chem Soc.* 2020;142(42):17828–17844.
- 7. Nishida K, Sato H, Oketani R, Mochizuki K, Temma K, Kumamoto Y, Tanaka H, Fujita K. Using saturated absorption for superresolution laser scanning transmission microscopy. *J Microsc.* 2021; https://doi.org/10.1111/jmi.13033
- 8. Masihzadeh O, Schlup P, Bartels RA. Enhanced spatial resolution in third-harmonic microscopy through polarization switching. *Opt Lett.* 2009;34(8):1240–1242.
- 9. Field JJ, Wernsing KA, Domingue SR, Allende Motz AM, DeLuca KF, Levi DH, DeLuca JG, Young MD, Squier JA, et al. Superresolved multiphoton microscopy with spatial frequency-modulated imaging. *Proc Natl Acad Sci USA*. 2016;113(24):6605–6610.
- 10. Pawlowska M, Tenne R, Ghosh B, Makowski A, Lapkiewicz R. Embracing the uncertainty: the evolution of SOFI into a diverse family of fluctuation-based super-resolution microscopy methods. *J Phys Photonics*. 2021;4(1):012002.
- Mangeat T, Labouesse S, Allain M, Martin E, Poincloux R, Bouissou A, Cantaloube S, Courtaux E, Vega E, Li T, et al. Super-resolved live-cell imaging using random illumination microscopy. *Cell Rep Methods*. 2021;1(1):100009.
- 12. Michler P, Imamoğlu A, Mason MD, Carson PJ, Strouse GF, Buratto SK. Quantum correlation among photons from a single quantum dot at room temperature. *Nature*. 2000;406(6799):968–970.
- 13. Dertinger T, Colyer R, Iyer G, Weiss S, Enderlein J. Fast, background-free, 3d super-resolution optical fluctuation imaging (SOFI). *Proc Natl Acad Sci USA*. 2009;106(52):22287–22292.
- Schwartz O, Oron D. Improved resolution in fluorescence microscopy using quantum correlations. *Phys Rev A*. 2012;85(3):033812.
- Lounis B, Bechtel HA, Gerion D, Alivisatos P, Moerner WE. Photon antibunching in single CdSe/ZnS quantum dot fluorescence. *Chem Phys Lett.* 2000;329(5–6):399–404.
- Schwartz O, Levitt JM, Tenne R, Itzhakov S, Deutsch Z, Oron D. Superresolution microscopy with quantum emitters. *Nano Lett.* 2013;13(12):5832–5836.
- 17. Gatto Monticone D, Katamadze K, Traina P, Moreva E, Forneris J, Ruo-Berchera I, Olivero P, Degiovanni IP, Brida G, Genovese M. Beating the abbe diffraction limit in confocal microscopy via nonclassical photon statistics. *Phys Rev Lett.* 2014;113(14):143602.
- 18. Israel Y, Tenne R, Oron D, Silberberg Y. Quantum correlation enhanced super-resolution localization microscopy enabled by a fibre bundle camera. *Nat Commun.* 2017;8(1):14786.
- Tenne R, Rossman U, Rephael B, Israel Y, Krupinski-Ptaszek A, Lapkiewicz R, Silberberg Y, Oron D. Super-resolution enhancement by quantum image scanning microscopy. *Nat Photonics*. 2019;13(2):116–122.
- Rossman U, Tenne R, Solomon O, Kaplan-Ashiri I, Dadosh T, Eldar YC, Oron D. Rapid quantum image scanning microscopy by joint sparse reconstruction. *Optica*. 2019;6(10):1290–1296.
- Lubin G, Tenne R, Antolovic IM, Charbon E, Bruschini C, Oron D. Quantum correlation measurement with single photon avalanche diode arrays. *Opt Express*. 2019;27(23):32863–32882.
- Futia G, Schlup P, Winters DG, Bartels RA. Spatially-chirped modulation imaging of absorbtion and fluorescent objects on single-element optical detector. *Opt Express*. 2011;19(2):1626–1640.

- 23. Winters DG, Bartels RA. Two-dimensional single-pixel imaging by cascaded orthogonal line spatial modulation. *Opt Lett.* 2015;40(12):2774–2777.
- 24. Stockton PA, Field JJ, Bartels RA. Single pixel quantitative phase imaging with spatial frequency projections. *Methods*. 2018;136:24–34.
- Stockton PA, Field JJ, Squier J, Pezeshki A, Bartels RA. Single-pixel fluorescent diffraction tomography. Optica. 2020;7(11):1617–1620.
- Stockton P, Murray G, Field JJ, Squier J, Pezeshki A, Bartels RA. Tomographic single pixel spatial frequency projection imaging. Opt Commun. 2022;520:128401.
- 27. Classen A, von Zanthier J, Scully MO, Agarwal GS. Superresolution via structured illumination quantum correlation microscopy. *Optica*. 2017;4(6):580–587.
- 28. Worts N, Czerski J, Jones J, Field JJ, Bartels R, Squier J. Simultaneous multi-dimensional spatial frequency modulation imaging. *Int J Optomechatronics*. 2020;14(1):1–17.
- 29. Heuke S, Sivankutty S, Scotte C, Stockton P, Bartels RA, Sentenac A, Rigneault H. Spatial frequency modulated imaging in coherent anti-stokes raman microscopy. *Optica*. 2020;7(5):417–424.